ELSEVIER

Journal of Alloys and Compounds 303–304 (2000) 505–508

Journal of ALLOYS AND COMPOUNDS

www.elsevier.com/locate/jallcom

Magnetic phase diagram of flux-grown single crystals of CeSb

T.A. Wiener*, P.C. Canfield

Ames Laboratory and Department of Physics and Astronomy, Iowa State University, Ames, IA 50011, USA

Abstract

CeSb is well known for having a particularly complex $H-T$ phase diagram. Most of the studies on this compound have been performed on crystals produced by a direct reaction technique. Here, we report on crystals of CeSb grown from a high temperature melt utilizing a third element, in this case tin, as a flux. The crystals are of exceptionally high quality, having a residual resistance ratio $\rho(300\ \mathrm{K})/\rho(2\ \mathrm{K}) > 400$. We present detailed magnetization and resistivity data performed in order to map the $H-T$ phase diagram which has never been fully determined by thermodynamic and transport measurements. The resulting phase diagram is exceptionally complex, corresponds well with the results of neutron scattering studies, and reveals at least two new ordered states.

Keywords: Magnetically ordered materials; Crystal growth; Electronic transport; Magnetization; Phase diagrams

1. Introduction

Cerium monoantiminide is a well-known example of a system with a complex magnetic phase diagram, with up to 14 distinct metamagnetic states [1]. Many studies have been done over the past three decades in order to better understand the nature of these states. Currently, it is understood that these states are made up of stacks of ferromagnetic planes. Each state has a particular stacking order of ferro- and antiferromagnetically aligned layers intermixed with paramagnetic layers [2,3]. Most of these studies have been done on crystals grown from a direct reaction method [4,5]. This technique produces relatively small crystals [5], though larger crystals have been reported [6]. In this paper we present data on crystals grown from a tin flux. The results of magnetic and transport measurements on these crystals indicate that these crystals are well formed and of high purity and allow for the determination of the full $H-T$ phase diagram from just thermodynamic and transport measurements.

2. Experimental methods

Crystals of CeSb were grown from a high temperature melt utilizing a third element, in this case tin, as a flux [7]. The elements Ce (Ames Laboratory, 99.99%), Sb (Aesar, 99.99%) and Sn (Aesar, 99.99+%) were placed in an alumina crucible with an atomic ratio of $(CeSb)_{0.06}Sn_{0.94}$. The crucible was then sealed in a partial pressure of argon in a quartz ampoule. The melt was heated to 1150°C, then slowly cooled over a period of 115 h to 800°C, at which temperature the excess flux was decanted from the crystals. Crystals of CeSb grown in this manner have a cubic morphology with an average cube side of 5 mm and mass of approximately 60 mg.

Dc magnetization measurements were performed with a Quantum Design SQUID magnetometer. A single crystal of approximately 40 mg was aligned with the (001) direction parallel to the applied field. Measurements of dc magnetization as a function of increasing applied field from 0 to 55 000 Oe were performed at several temperatures and as a function of increasing temperature at several fields.

The electrical resistivity was measured using a standard four-probe technique with an ac bridge operating at 16 Hz, and using current densities of between 0.1 and 1.0 A/cm^2. Electrical contact was made to the samples using Epo-tek H20E silver epoxy, with typical contact resistances of about 4 Ω. Due to the uncertainty of the bar dimensions and the contact separation, there is an approximate uncertainty of ±10% in absolute values of the resistivity. The sample used for resistivity measurements was easily cleaved from a larger crystal and had dimensions of $1.6\times 0.31\times 0.03\ mm^3$. Resistivity as a function of increasing

*Corresponding author. Tel.: +1-515-294-9772.
E-mail address: twiener@iastate.edu (T.A. Wiener)

0925-8388/00/$ – see front matter
PII: S0925-8388(00)00636-8

field and as a function of increasing temperatures was measured at several temperatures and fields, respectively.

3. Results and discussion

The dc susceptibility χ at 1000 Oe (where χ is defined as M/H at low fields) is shown in Fig. 1. The dc susceptibility at temperatures well above the Neel temperature is well fitted by the Curie–Weiss law, $\chi = C/(T-\theta)$, which is demonstrated by linearity of the inverse dc susceptibility at temperatures above the Neel temperature (Fig. 1, inset). From this it is determined that $p_{\text{eff}} = 2.51$, which is very close to the trivalent cerium value of 2.54, and the Weiss temperature $\theta = +8.9$ K is comparable to values reported elsewhere [4,5], and indicates a competition between ferromagnetic interactions and the antiferromagnetic ordering that takes place at the Neel temperature $T_N = 16.7$ K.

The zero field resistivity is shown in Fig. 2. The temperature dependence of the resistivity is relatively flat at high temperatures with a room temperature value of 100 $\mu\Omega$ cm. There is a large loss of spin disorder scattering below the Neel temperature of 16.7 K, which leads to a resistivity of 0.24 $\mu\Omega$ cm at 2 K. The residual resistivity ratio ($\rho_{300\text{ K}}/\rho_{2\text{ K}}$) is 415, which is an order of magnitude higher than previously reported [5]. As will be shown below, it is the low residual resistivity of these samples that allows for the detection of many of the magnetic transitions through transport measurements.

Fig. 1 shows the low temperature dc susceptibility in detail. Several magnetic transitions can be seen. The transition temperatures were determined from the peaks in $\mathrm{d}(\chi T)/\mathrm{d}T$, which is considered to be proportional to the magnetic component of the specific heat near an antiferromagnetic transition [8] (Fig. 3). Many of these same transitions can be seen in the low temperature resistivity (Fig. 2, inset). In this case the transition temperatures are determined from the peaks in $\mathrm{d}\rho/\mathrm{d}T$ (Fig. 3). The Neel temperature is the same for both of these measurements and is $T_N = 16.7$ K, which is in good agreement with previous work. Note that the transitions at 8 and 12.2 K, which are apparent in the magnetization measurement, are not seen in the resistivity.

The dc magnetization as a function of applied field at 5 K is shown in Fig. 4. The saturated moment $p_{\text{sat}} = 1.98$ at 5.5 T, which is close to the value of 2.14 for trivalent cerium. Several metamagnetic transitions can readily be seen and the critical fields for these transitions were determined from the peaks in $\mathrm{d}M/\mathrm{d}H$. The resistivity as a function of field at 5 K also reveals these transitions, critical fields from which were determined from the peaks

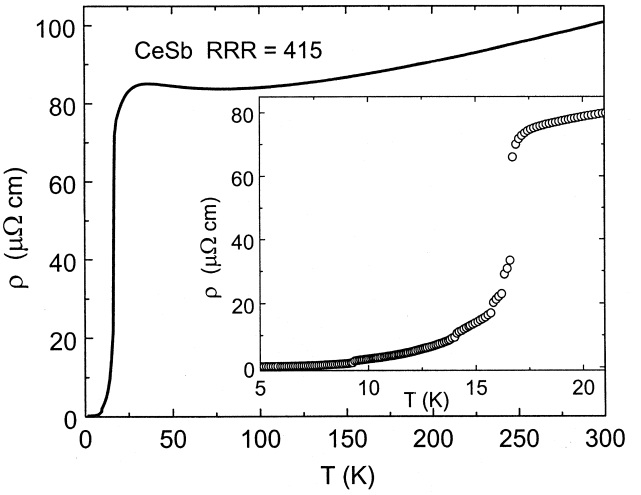

Fig. 2. Resistivity as a function of temperature in zero field. Inset shows expanded view of low temperature region.

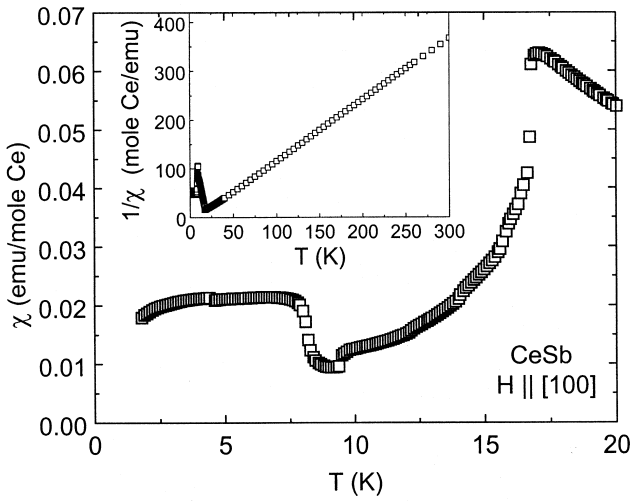

Fig. 1. Dc susceptibility of CeSb as a function of temperature at $H = 1$ kOe. Inset shows the inverse susceptibility as a function of temperature at 1 kOe.

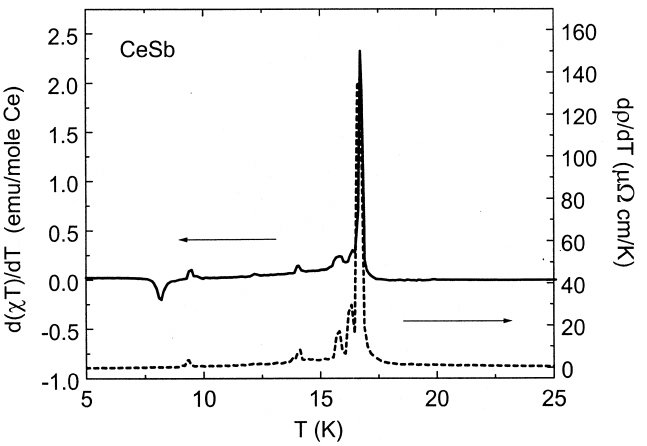

Fig. 3. $\mathrm{d}(\chi T)/\mathrm{d}T$ at 1 kOe as a function of temperature (———, left-hand axis) and $\mathrm{d}\rho/\mathrm{d}T$ at 0 kOe as a function of temperature (- - -, right-hand axis).

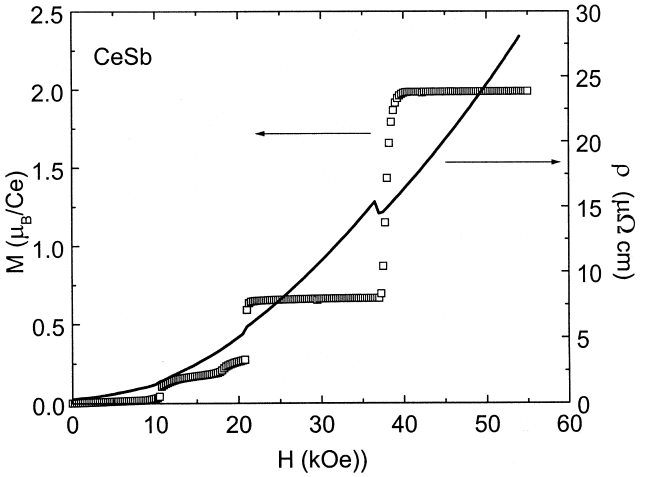

Fig. 4. Magnetization as a function of applied field (□, left-hand axis) and resistivity as a function of applied field (———, right-hand axis) at 5 K.

in $d\rho/dH$. In addition, there is a relatively large magnetoresistance with $(\rho(H) - \rho(0))/\rho(0) = 9000\%$ at 55 kOe. This is comparable to the magnetoresistance seen in other high purity, semimetallic antimony intermetallics [9,10].

Using a total of 29 isothermal $M(H)$ and $\rho(H)$ runs and 29 constant field $M(T)$ and $\rho(T)$ runs a magnetic phase diagram was constructed (Fig. 5). This phase diagram compares very well with those that have been reported previously [2,5,11,12]. These states can be identified with the states described by specific heat and neutron measurements [2]. Most of the states can be differentiated from the resistivity measurements and all of them by the magnetization measurements. Fig. 5b shows an expanded view of a portion of the phase diagram. It should be noted that the three transitions around 16 K are clearly distinguished by both measurements. Ref. [1] states that previous magnetization measurements were unable to resolve the majority of the low field states. In addition, previous transport measurements, though able to discern the high temperature, low field states, were unable to distinguish the low temperature, low field states clearly [5], nor were these transitions seen in all samples. This was attributed to differences in sample quality. That all the phases can be detected in our samples by thermodynamic and transport measurements confirms that crystals of CeSb grown from a tin flux are of a higher quality than previously grown samples.

In addition to resolving all the known phases in the $H–T$ phase diagram, several new states are also seen. These new states appear between states FP1 and FP2, between FP2 and FP3, and between AFF2 and AFF1 (where states are labeled as described in Ref. [2]). Although these phases exist over a small region of $H–T$ space they are clearly resolved in both $M(T)$ and $\rho(T)$ data. Fig. 6a shows $M(T)$ and $\rho(T)$ for $H = 30$ kOe. The two pairs of arrows indicate

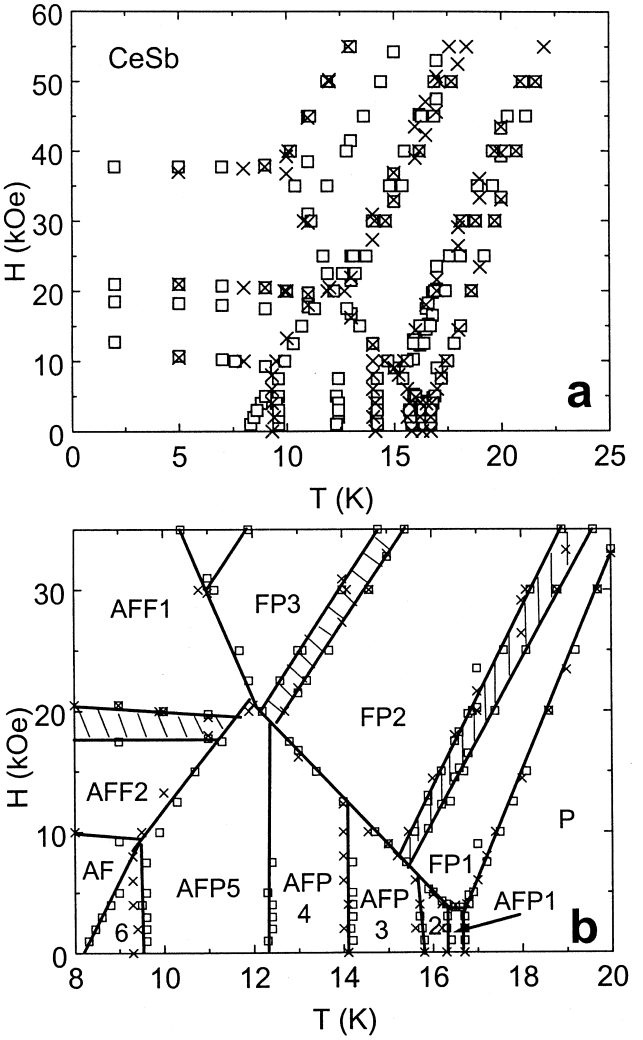

Fig. 5. (a) Total $H–T$ phase diagram constructed as described in text. (□) Determined from magnetization data; (×) determined from resistivity data. (b) Expanded view of phase diagram. Lines were added as a guide to the eye. States are labeled as described in Ref. [2]. Potential new phases are shown as hatched.

the boundaries of these phases. This is also clearly seen in the temperature derivatives in Fig. 6b.

In conclusion, crystals of CeSb grown from a tin flux have a higher sample quality than that seen in previous samples. This has allowed the entire $H–T$ phase diagram to be mapped from bulk magnetization and resistivity measurements.

Acknowledgements

Ames Laboratory is operated for the U.S. Department of Energy by Iowa State University under contract No. W-7405-Eng-82. The Director for Energy Research, Office of Basic Energy Sciences, supported this work.

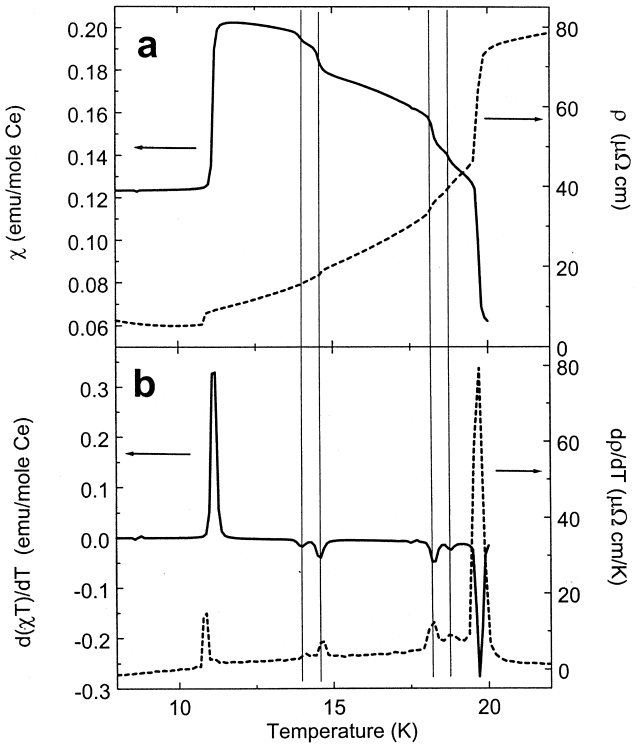

Fig. 6. (a) Dc susceptibility (———, left-hand axis) and resistivity (- - -, left-hand axis) as a function of temperature at 30 kOe. (b) $d(\chi T)/dT$ (———, left-hand axis) and $d\rho/dT$ (- - -, right-hand axis) at 30 kOe as a function of temperature. In both panels, vertical arrows highlight the boundaries of proposed new phases as described in text.

References

[1] O. Vogt, K. Mattenberger, Physica B 215 (1995) 22.
[2] J. Rossat-Mignod, P. Burlet, H. Bartholin, O. Vogt, R. Lagnier, J. Phys. C: Solid State Phys. 13 (1980) 6381.
[3] B. Lebech, K. Clausen, O. Vogt, J. Phys. C: Solid State Phys. 13 (1980) 1725.
[4] G. Busch, O. Vogt, Phys. Lett. 20 (1966) 152.
[5] M. Escorne, A. Mauger, D. Rovot, J.C. Achard, J. Phys. C: Solid State Phys. 14 (1981) 1821.
[6] P. Fischer, B. Lebech, G. Meier, B.D. Rainford, O. Vogt, J. Phys. C: Solid State Phys. 11 (1978) 345.
[7] P. Canfield, Z. Fisk, Philos. Mag. B 65 (1992) 1117.
[8] M. Fischer, Philos. Mag. 7 (1962) 1731.
[9] S. Bud'ko, P. Canfield, C. Mielke, A. Lacerda, Phys. Rev. B 57 (1998) 13624.
[10] K. Myers, S. Bud'ko, I. Fisher, Z. Islam, H. Kleinke, P. Canfield, A. Lacerda, J. Magn. Magn. Mater. (in press).
[11] G. Meier, P. Fischer, W. Halg, B. Lebech, B.D. Rainford, O. Vogt, J. Phys. C: Solid State Phys. 11 (1978) 1173.
[12] H. Bartholin, D. Florence, W. Tcheng-si, O. Vogt, Phys. Status Solidi (a) 29 (1975) 275.